# Dalton Transactions

Accepted Manuscript






ROYAL SOCIETY OF CHEMISTRY

www.rsc.org/dalton

Dalton Transactions

ARTICLE

# New tetranuclear manganese clusters with $[Mn^{II}_3Mn^{III}]$ and $[Mn^{II}_2Mn^{III}_2]$ metallic cores exhibiting the low and high spin ground state

Received 00th January 20xx,
Accepted 00th January 20xx

DOI: 10.1039/x0xx00000x

www.rsc.org/

M. Sobocińska,[a]* M. Antkowiak,[b] M. Wojciechowski,[c] G. Kamieniarz,[b] J. Utko[a] and T. Lis[a]

Two tetranuclear mixed-valent clusters, $[Mn^{II}_3Mn^{III}Cl(Ph_3CCOO)_4(CH_3OCH_2CH_2O)_4(CH_3CN)]\cdot 0.4C_6H_5CH_3\cdot 0.6CH_3CN$ (**1**) with unprecedented $[Mn^{II}_3Mn^{III}]$ core and $[Mn^{II}_2Mn^{III}_2Cl_4(CH_3OCH_2CH_2O)_6]$ (**2**) were synthesized and characterized by single-crystal X-ray diffraction, magnetic measurements and their properties were analyzed in the framework of phenomenological modelling as well as DFT calculations, yielding the acceptable agreement between theory and experiment. Both building blocks $[Mn^{II}_3Mn^{III}]$ and $[Mn^{II}_2Mn^{III}_2]$ provide good examples of bipartite systems with the lowest $S_T$=1/2 and the highest $S_T$=9 magnetic ground states available for them. It is demonstrated that the topology of the magnetic interactions in the $[Mn^{II}_3Mn^{III}]$ core provides a suitable template for the molecular qubit implementation and the stability of the spin-1/2 ground state strongly depends on the antiferromagnetic $Mn^{II}$ – $Mn^{II}$ coupling.

## Introduction

The chemistry of manganese raises an interest, since there is a possibility of creating polynuclear clusters containing manganese ions on mixed-valent oxidation states.[1] These compounds with metals having unpaired electrons in the 3d shell can have attractive magnetic properties, that may lead to the potential application in information storage at nano-level.[2] Since 1993, when the group of Gatteschi elucidated the unacknowledged slow magnetic relaxation behaviour of the molecule $[Mn_{12}(CH_3COO)_{16}(H_2O)_4O_{12}]\cdot 2CH_3COOH\cdot 4H_2O$ below the blocking temperature, the investigation on single-molecule magnets (SMMs) has begun.[3] This discovery led scientists to build up new paths of synthesis in order to obtain materials exhibiting similar features with higher blocking temperature or the diminished quantum tunnelling of the magnetization through the energy barrier.[4] Along this line of research, a number of tetranuclear manganese clusters ($Mn_4$ in short) showing the slow magnetic relaxation has been synthesized and characterized.[5a-e,6g]

There is also an effort to synthesize molecular nanomagnets for quantum information processing with the ground state S=1/2 representing the molecular qubits.[6a-c] The prerequisites for this type of features is the odd number of half-integer spins and a sizable energy gap between the ground and the first excited state. So far it has been realized in a family of the chromium based rings.[6a-c] In the vast list of the $Mn_4$ complexes collected[6d] only that denoted $Mn^{II}Mn^{III}_3$ (M.W. Wemple et al.[6e] fulfils the first criterion but its ground state determined by the interaction parameters does not belong to the S=1/2 sector.

Another area of interest in small polynuclear mixed-valent clusters is an experimental verification of the fundamental Lieb-Mattis theorem (LMT) which predicts the ground states in the bipartite spin systems.[6g-h] The essential role of the system bipartiteness has been recently recognized in relation to spin frustration in molecular nanomagnets.[6b-c,6i-j] The existing and new molecular materials containing $Mn_4$ cores may become the test beds for validation of LMT which in turn may predict a proper ground state in a given sector of the interaction parameters.[7]

Furthermore, the suitable clusters with four manganese ions in the structure can act as a key to explain still unsolved mystery of water-splitting, taking place in Photosystem II, located in the thylakoid membranes of the oxygenic photosynthetic organisms.[8] The active centre where a light-induced process leads to creation of an O–O bond in this protein complex, is formed by four manganese ions (two Mn(III) and two Mn(IV)) and one calcium ion, connected via oxygen bridging atoms ($Mn_4CaO_5$).[9a] Recent research has determined more exact structure of PSII obtained from data coming from a femtosecond X-ray free electron laser (XFEL), what provided

[a] Faculty of Chemistry, University of Wrocław, Joliot-Curie 14, 50-383, Wrocław, Poland. E-mail: maria.sobocinska@chem.uni.wroc.pl
[b] Faculty of Physics, A. Mickiewicz University, Umultowska 85, 61-614, Poznań, Poland
[c] Institute of Physics, University of Zielona Góra, Szafrana 4a, 65-516 Zielona Góra, Poland

†Electronic Supplementary Information (ESI) available. CCDC 1437035, 1437036. For ESI and crystallographic data in CIF see DOI: 10.1039/x0xx00000x

important clue to the mechanism of water oxidation.[9b] Current knowledge of the structure of oxygen-evolving complex (OEC) inspires chemists to create adequate manganese compounds that could be used as catalysts in the process of splitting of the water molecule without using a lot of energy.

Hence the class of the tetranuclear manganese complexes containing the $[Mn_4(\mu_3–O)_2]$ moiety is attractive and has been widely studied.[10] The prime example of a mixed-valent cluster with $[Mn^{II}_2Mn^{III}_2(\mu_3–O)_2]^{6+}$ central core was reported in 1999[11] and since this time the continuation of searching for its analogues has led to several dozen structures published.[5a-e,12a-l,] In the "butterfly" structures, the body is often formed by the trivalent manganese ions, whereas the wings by the divalent manganese ions. However, the distribution of oxidation states has been changed so that there are examples of "reversed" cores with the $Mn^{II}$ ions replaced by the $Mn^{III}$ ions and vice versa[13a-c] and those with a rare $[Mn^{II}_2Mn^{IV}_2((\mu_3–O)_2]^{10+}$ core.[6d] The above-mentioned interesting structural features of polynuclear compounds and their role in molecular magnetism encouraged us to explore the reactions leading to creation of the tetranuclear mixed-valent manganese clusters with the even and odd number of $Mn^{II}$ ions carrying the half-integer spin.

In this paper we present the structure and magnetic properties of new manganese "butterfly" clusters with two different distributions of the oxidation states on the metallic centres: $[Mn^{II}_3Mn^{III}Cl(Ph_3CCOO)_4(CH_3OCH_2CH_2O)_4(CH_3CN)]\cdot0.4C_6H_5CH_3\cdot0.6CH_3CN$ (**1**) and $[Mn^{II}_2Mn^{III}_2Cl_4(CH_3OCH_2CH_2OH)4]$ (**2**). According to our best knowledge, a $[Mn^{II}_3Mn^{III}]$ core is unique as far as its composition and its ground state with the total spin $S_T$=1/2 are concerned. Both compounds provide non-trivial examples of the bipartite systems[7] and illustrate the LMT consequences.[6g-h]

## Experimental

The output complex $[Mn^{II}_4Cl_4(CH_3OCH_2CH_2O)_4(CH_3OCH_2CH_2OH)_3]_2$ was prepared as previously described.[14] The solvents (toluene, acetonitrile and ethanol) were distilled under dinitrogen from the appropriate drying agents. Triphenylacetic acid and 2-methoxyethanol were purchased from Sigma Aldrich and used as received. Elemental analyses (C, H, N) were performed on a vario EL III Elementar element analyzer. To determine an amount of chlorine atoms in both complexes the following method was used: the sample was burned in oxygen in micro K apparatus. Solution of 5 ml $H_2O_2$ and 4 droplets of NaOH was placed in the steam of chlorine and it was left for next 2 hours to absorb Cl. $HNO_3$ was added to maintain pH around 2-3. After that, 1,5-diphenylcarbazone was added to the mixture and the titration was carried out (0.005 M mercury perchlorate was used as a titrant). The titration was finished when the color of solution became violet. Elemental analysis of Mn and Na was carried out on atomic absorption spectrometer SOLAAR M6 Mk2.

**Synthesis of $Ph_3CCOONa$.** The reaction and every operation was performed under inert atmosphere using standard Schlenk techniques. At first 20 $cm^3$ ethanol was added to the stirring mixture of metallic sodium (0.801 g, 34.83 mmol), triphenylacetic acid (10.00 g, 34.69 mmol) and 200 $cm^3$ toluene in order to obtain sodium ethanolate that reacted with triphenylacetic acid, giving white precipitation of $Ph_3CCOONa$. Then the white solid product was washed in toluene, collected by filtration and dried in vacuum. Yield: 5.24 g (48.25 %). Anal. calcd (%) for $C_{20}H_{15}O_2Na$: C 77.41, H 4.87, Na 7.41; found: C 77.36, H 4.90, Na 7.40.

**Synthesis of $[Mn^{II}_3Mn^{III}Cl(Ph_3CCOO)_4(CH_3OCH_2CH_2O)_4(CH_3CN)]\cdot0.4C_6H_5CH_3\cdot0.6CH_3CN$ (1).** Synthesis was performed under a dry nitrogen atmosphere using standard Schlenk techniques. The chemical reaction of the cubane-type octanuclear manganese(II) complex[14] $[Mn^{II}_4Cl_4(CH_3OCH_2CH_2O)_4(CH_3OCH_2CH_2OH)_3]_2$ (2.816 g, 12.66 mmol) with anhydrous $Ph_3CCOONa$ (2.697 g, 8.43 mmol) in the mixture of 20 $cm^3$ $CH_3CN$ and 45 $cm^3$ $C_6H_5CH_3$ was carried out in 65 $^oC$ under nitrogen atmosphere. After one hour of stirring, an access to air was allowed. After three hours the heating was stopped. After three days of mixing the solution, when its colour was changed into red-brown, it was concentrated and then filtered. The mass of solid was 0.490 g (theoretical mass of NaCl for this reaction is 0.493 g). Two weeks later single crystals of complex **1** suitable for X-ray diffraction were obtained. Color: dark brown. Yield: 0.512 g (50.4%). Anal. calcd (%) for $C_{98}H_{96}N_{1.6}ClMn_4O_{16}$: C 65.07, H 5.31, N 1.24, Cl 1.96, Mn 12.16; found: C 65.12, H 5.35, N 1.29, Cl 2.07, Mn 12.15.

**Synthesis of $[Mn^{II}_2Mn^{III}_2Cl_4(CH_3OCH_2CH_2O)_6]$ (2).** The second compound was obtained due to a simple oxidation of the complex $[Mn^{II}_4Cl_4(CH_3OCH_2CH_2O)_4(CH_3OCH_2CH_2OH)_3]_2$.[14] A Schlenk flask containing crystals of this octanuclear manganese(II) complex in the mixture of 2-methoxyethanol and toluene was left opened for two weeks. It led to precipitation of the red crystals of complex **2**. Color: red. Anal. calcd (%) for $C_{18}H_{42}Cl_4Mn_4O_{12}$: C 26.62, H 5.21, Cl 17.46, Mn 27.06; found: C 26.71, H 5.23, Cl 17.42, Mn 27.07.

**Single-crystal X-ray diffraction.** Diffraction data for **1** were collected at 100(2) K on an Agilent Xcalibur PX KM-4-CCD four circle difractometer using Mo-Kα radiation (λ = 0.71073 Å). Diffraction data for **2** were collected at 100(2) K on Xcalibur single crystal diffractometer with CCD camera, using Mo-Kα radiation. The CrysAlisPro software package of Oxford Diffraction was used for cell refinements, data reductions and absorption corrections.[15] Analytical absorption corrections were applied using a multifaceted crystal model.[16] The structures were solved by direct methods (SHELXS97)[17] and refined by full matrix least-square techniques on $F^2$ with SHELXL2013.[18] All non-hydrogen atoms were refined with anisotropic thermal parameters. All H atoms were treated as riding on their parent atoms and assigned isotropic temperature factors: $U_{iso}(H) = 1.5U_{eq}(C)$ (methyl) and $U_{iso}(H)$ =

Dalton Transactions

ARTICLE

$1.5U_{eq}$(C) (non-methyl). The unbound acetonitrile and toluene in **1** were modeled as disordered over an inversion centre. Moreover, these molecules were refined as partially occupied with the occupancies of 0.6 and 0.4 for acetonitrile and toluene, respectively. Carbon atoms in phenyl ring were fitted to a regular hexagon by using an AFIX 66 command. The crystallographic data for **1** and **2** are given in Table S1 and some of the crystallographic details such as selected bond lengths are summarized in Table S2 and S6 in the ESI. CCDC 1437035 (**1**) and 1437036 (**2**) contain detailed crystallographic data for this paper.

**Magnetic data collection.** Magnetic measurements in the temperature range 1.8-300 K for **1** and **2** were carried out on powdered samples, at the magnetic field 0.5 T using the Quantum Design SQUID-based MPMS XL-5-type Magnetometer. Corrections for diamagnetism were applied to the observed paramagnetic susceptibility using Pascal's constants.[19] Magnetization measurements were conducted at 2 K in the magnetic field from 0 to 5.0 T. Alternating current magnetic susceptibility measurements were performed on a polycrystalline samples of complexes **1** and **2** in the 2-10 K range in zero applied field and a 3 Oe ac field oscillating at 10-1500 Hz. The frequency dependence out-of-phase ($\chi_M''$) signals were not observed for both complexes, therefore these results are not referred to hereafter.

## Results and discussion

### Description of the structures

Single crystal X-ray analysis reveals that complex **1** crystalizes in the monoclinic crystal system with the space group *P2₁/n*. Selected interatomic distances are collected in Table S2. The crystallographic asymmetric unit contains one tetranuclear molecule of $[Mn^{II}_3Mn^{III}Cl(Ph_3CCOO)_4(CH_3OCH_2CH_2O)_4(CH_3CN)]$ shown in Fig. 1. Apart from tetranuclear clusters, the unit cells contain also disordered molecules of solvents. Acetonitrile and toluene exhibit two types of disorder: positional and substitutional. They are located in the same site and on the inversion centre as well. The occupancies are 0.4 and 0.6 for $CH_3CN$ and $C_6H_5CH_3$, respectively. The tetranuclear metallic core contains a $[Mn^{II}_3Mn^{III}O_4]^+$ cationic unit, where Mn1 is $Mn^{3+}$, but Mn2, Mn3 and Mn4 are $Mn^{2+}$. Each Mn3 triangular unit is bridged by $\mu_3$–O oxygen atoms (O1N, O1P) of 2-methoxyethanolate ligands displaying a $\kappa^1{:}\kappa^1{:}\mu^3$ coordination mode. Additionally, two kinds of connections between outer manganese pairs can be distinguished. The first two pairs, Mn1/Mn2 and Mn1/Mn3, are bridged by carboxylate arms of triphenylacetate ligands and by $\mu_2$–O oxygen atoms (O1O, O1M) of 2-methoxyethanolate ligands representing $\kappa^1{:}\kappa^1{:}\mu^2$ mode, as well as by $\mu_3$–O oxygen atoms (O1N, O1P) of 2-methoxyethanolate ligands representing $\kappa^1{:}\kappa^1{:}\mu^3$ mode. It needs to be mentioned that all bidentate triphenylacetate ligands present in the structure are found in the usual $\kappa^1{:}\kappa^1{:}\mu^2$ coordination mode. The second two pairs, Mn2/Mn4 and Mn3/Mn4, are bridged by triphenylacetate ligands and $\mu_3$–O oxygen atoms (O1N, O1P) from 2-methoxyethanolate ligands. Oxidation states were determined on the grounds of bond valence calculation (Table S3),[20] structural and charge considerations. Mn1 atom shows an evidence for Jahn-Teller distortion, as expected for high-spin octahedral $Mn^{3+}$ ion with $d^4$ configuration. The elongation occurs along O1C-Mn-O1N (Table S2). The geometry of the complex could be described as a distorted "butterfly" with Mn1 and Mn4 ions indicating the body, whereas Mn2 and Mn3 ions are located on the wings. Interestingly, this is not typical $Mn_4$ "butterfly" structure known in literature.[21] In the first place the oxidation states are uncommon and the charge distribution found in the metallic core has not been encountered yet. Secondarily, the dicubane-like geometry is shattered, because of triphenylacetate ligands, that connect body manganese ions with wing-tip manganese ions via three atoms: O–C–O, instead of one bridging atom. Alternatively, in this structure we can consider metallic core with the $[Mn^{II}_3Mn^{III}]^{9+}$ *non-planar unit*. Then, if we find three picked manganese ions lying on the common plane, the fourth manganese ion is located within less than 1 Å perpendicularly to this plane. It is worth mentioning that in the complexes with general "butterfly" geometry all metallic ions lie on the common plane. In the discussed structure *every manganese ion has different chemical environment*. Atoms: Mn1 ($d^4$ configuration) and Mn2 are six-coordinated with consecutively: $\{O_6\}$ and $\{O_5Cl\}$ coordination spheres, adopting distorted octahedral geometry. In the coordination sphere of Mn3 atom, the distance Mn3–O2P equals to 2.5553(6) Å. Such long Mn–O bonds are scarce. Search for structures with Mn–O bonds was performed in ConQuest (14th July 2015) and the lengths of bonds between oxygen atoms coordinated to manganese atoms were analyzed.[22] Among 9826 results, only 394 matched to the compounds containing Mn–O bonds longer than 2.499 Å. In the complex **1** positions of six oxygen atoms and one nitrogen atom in the coordination sphere around Mn3 centre indicate *distorted pentagonal* bipyramidal geometry. The *distorted trigonal* bipyramidal coordination sphere of Mn4 comprises five O-atom donors creating $\{O_5\}$ arrangement.

The complex $[Mn^{II}_2Mn^{III}_2Cl_4(CH_3OCH_2CH_2O)_6]$ (**2**) drawn in Fig. 2 is also a tetranuclear species which crystallizes in the monoclinic *P2₁/c*

space group. Selected interatomic distances are collected in Table S6. Half of the centrosymmetric molecule lies in the crystallographic asymmetric unit. Face-shared dicubane-like metallic core without two opposite vertices is composed of $[Mn^{II}_2Mn^{III}_2O_6]^{4+}$ cationic unit, where six oxygen atoms come from six 2-methoxyethanolate ligands. In contrast to the complex **1**, the $[Mn^{II}_2Mn^{III}_2]^{4+}$ unit in **2** is *planar* rhombus, thus forming a typical "butterfly" complex. The bond lengths and charge distribution considerations as well as bond valence sum (BVS) calculation (Table S7) led to the conclusion that body manganese ions are $Mn^{3+}$ whereas two wing-type ions are $Mn^{2+}$. The coordination mode of six 2-methoxyethanolate ligands is achieved in two different ways. Two ligands have $\kappa^1:\kappa^1:\mu^3$ mode and their $\mu_3$–O atoms bridge two $[Mn^{II}Mn^{III}_2]^{8+}$ triangle units. The second representation $\kappa^1:\kappa^1:\mu^2$ occurs for four 2-methoxyethanolate ligands bridging $[Mn^{II}Mn^{III}]^{5+}$ units. All of the Mn ions are *six-coordinated with {$O_5Cl$} environment*: Mn1 has *distorted octahedral* geometry with two shorter and four longer bonds (Table S6), while Mn2 adopts *distorted trigonal* prismatic geometry. Geometric parameters related to the intra-molecular hydrogen-bond interactions are described for both complexes in Electronic Supplementary Information (Tables S4, S5, S8).

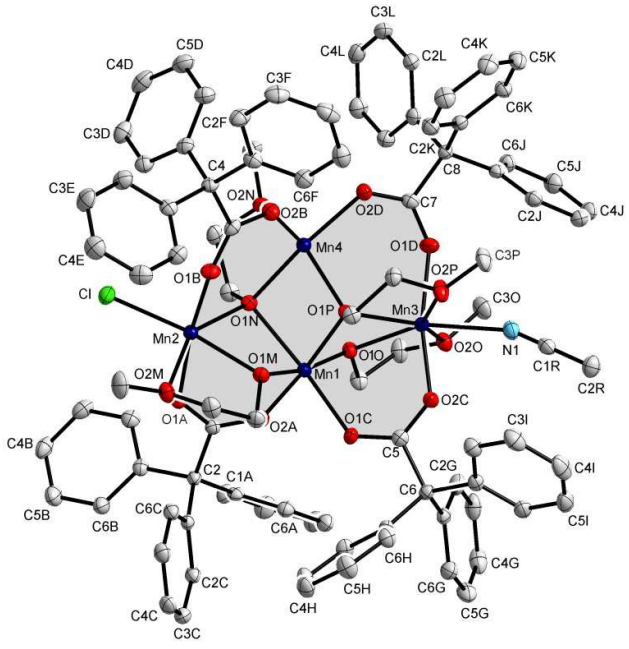


Fig. 1. The molecular structure of $[Mn^{II}_3Mn^{III}Cl(Ph_3CCOO)_4(CH_3OCH_2CH_2O)_4(CH_3CN)]$ (**1**), with displacement ellipsoids drawn at the 50% probability level. H atoms have been omitted for clarity.

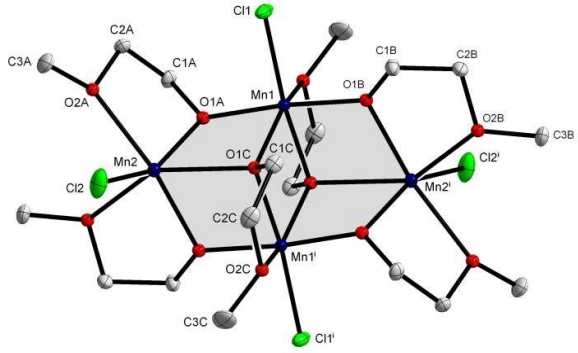


Fig. 2. The molecular structure of $[Mn^{II}_2Mn^{III}_2Cl_4(CH_3OCH_2CH_2O)_6]$ (**2**), with displacement ellipsoids drawn at the 50% probability level. H atoms have been omitted for clarity.

**Magnetic studies**

The magnetic properties of **1** and **2** have been analyzed in terms of the Heisenberg spin model. The structures of the Mn···Mn magnetic interactions are sketched in Fig. 3, where the red and blue circles represent the S=5/2-$Mn^{II}$ and S=2-$Mn^{III}$ ions, respectively. In addition, a rearrangement of labels is performed in Fig. 3 so that the Mn1 ions of **1** and **2** are located accordingly on the sites 3 and 1.

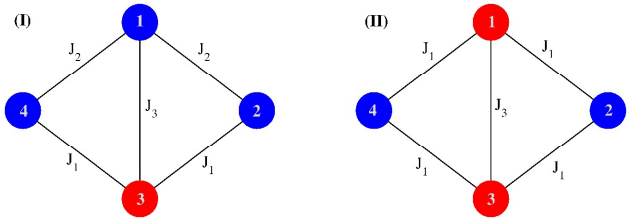


Fig.3. Schematic representation of the magnetic cores in **1** (panel I) and **2** (panel II). The blue and red circles with labels visualize the manganese $Mn^{II}$ and $Mn^{III}$ ions and their positions. The blue and red positions are occupied by spins S=5/2 and S=2, respectively.

Thus the corresponding Heisenberg Hamiltonians modelling the magnetic interaction in the complexes **1** and **2** are given by

$$H_1 = J_1(S_3 \cdot S_2 + S_3 \cdot S_4) + J_2(S_1 \cdot S_2 + S_1 \cdot S_4) + J_3 S_1 \cdot S_3 \quad (1)$$

and

$$H_2 = J_1(S_1 + S_3) \cdot (S_2 + S_4) + J_3 S_1 \cdot S_3 \quad (2)$$

respectively, where the notation follows that in Fig. 3. The model (1) is extremely simplified, in view of the complicated structure of **1** described in the preceding subsection, but more realistic model would lead to over-parameterization, taking into account that the bulk magnetometry measurements were performed on the powder sample.

The experimental temperature-dependent susceptibility results denoted by $\chi$ and the in-field magnetization isotherms measured on the powder sample at T=2 K for both tetranuclear structures **1** and **2** are drawn by the symbols in Figs. 4 -5 and Figs. 6 – 7,

Dalton Transactions

ARTICLE

respectively. They were fitted by the theoretical curves obtained for the models (1) and (2) within the numerically exact diagonalization technique.[23a-c] The temperature independent paramagnetism was fixed at 0, intermolecular interactions were taken into account on the mean-field level and the configuration averaging was performed if the zero-field splitting was imposed, having exploited the formulae (4.4) - (4.6) given by Boča.[24] We note that the constant $k_B$ is redundant in Eq. (4.5) therein and we have adopted the simplified notation, assuming J'= *zj*. The inverse susceptibility dependence on temperature is drawn in the insets of Figs. 4 and 5 and the extrapolations of the high temperature part yield the Weiss constant Θ equal to –38 K and 29 K for **1** and **2**, respectively. These values suggest the antiferro- and ferro-magnetic fluctuations in **1** and **2** which can be accounted for in the fitting procedure *via* the intermolecular couplings J'.

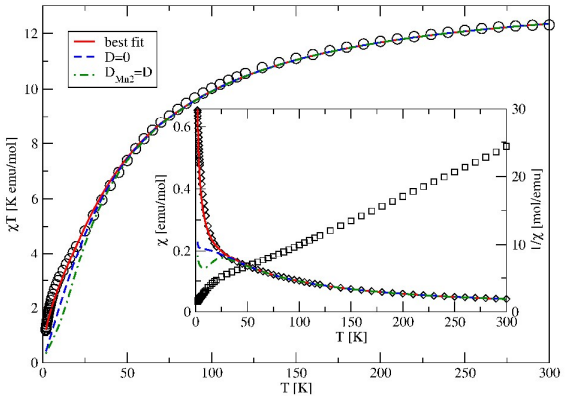


Fig. 4. Temperature dependence of the magnetic susceptibility of **1** as function of temperature. The symbols represent the experimental data: circles, diamonds and squares correspond to χT, χ and 1/χ, respectively. The theoretical curves are described in the legend. The best fit is achieved for the parameters given in Eq. (3).

We checked that for **1** the temperature dependence of χ in conjunction with the in-field magnetic moment isotherms could not be fitted quantitatively within the model (1), even if the terms with different values of the *g* factors and the uniaxial zero-field splitting parameters for the metallic centres were taken into consideration. This shortcoming can be attributed to the deficiency of our model to represent accurately enough the structure of the low-lying energy levels which is tuned by the applied field. Relying on the experimental data available, the model cannot be improved, without the overparametrization pitfall.

Our modelling was focused on the susceptibility curves and proceeded as follows. First we have used a single *g* factor in the Zeeman term and we have corrected the susceptibility within the molecular field approach. The fits achieved *without* the zero-field splitting are demonstrated in Figs. 4 and 5 by the broken blue lines. They provide the values of the magnetic couplings and the Landé factors. Next, to diminish the low temperature deviations which occur between theory and experiment in Figs. 4 and 5, the zero-field splitting term was included in the simplest uniaxial form and only one value of the anisotropy parameter *D* was allowed. In addition, the comparison with the magnetization isotherms plotted in Figs. 6 and 7 was taken into consideration. Figs. 5 and 7 demonstrate that for **2** the quantitative agreement is reached, using a single parameter *D* common for all the manganese ions. In the case of **1**, the improvement of the low temperature part of χ can only be achieved if the sign of the anisotropy parameter $D_{Mn4}$ is different from that of Mn2 and Mn3 (according to the notation in Fig. 1). Final results are presented, imposing $D_{Mn2}= D_{Mn3}$, $D_{Mn1}=0$ and $D_{Mn4}\equiv D = -D_{Mn2}$. Attempts to relax these constraints have not led to relevant improvement so that the quantitative modelling of **1** needs some extra terms beyond the uniaxial zero-field splitting. We remind that **1** is unique as far as the deformation of the metallic core from the planar structure and the diversity of the chemical environment for each magnetic centre are concerned.

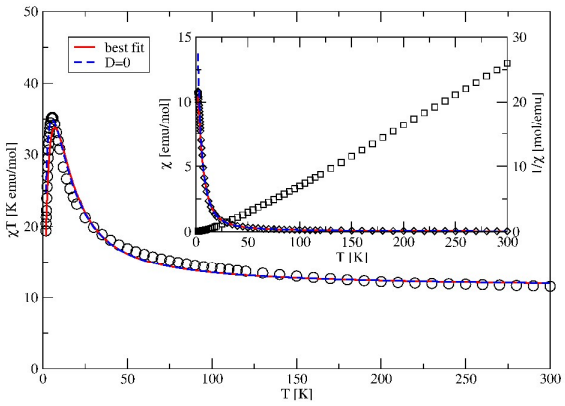


Fig. 5. The magnetic susceptibility of 2 as function of temperature. The experimental data are plotted by the same symbols as in Fig. 5. The parameters defining the best fit are given in Eq. (4).

The sets of the model parameters providing the best fit and expressed in the units of the Boltzmann constant $k_B$, are the following:

(a) for **1**

$J_1$=14.0 K, $J_2$=2.40 K, $J_3$=-2.7 K, $J'$=0.05 K

$D$=-4.5 K, $g$=1.90; (3)

(b) for **2**

$J_1$=-2.2 K, $J_3$=-7.4 K, $J'$=-0.06 K, $D$=3.0 K, $g$=1.70. (4)

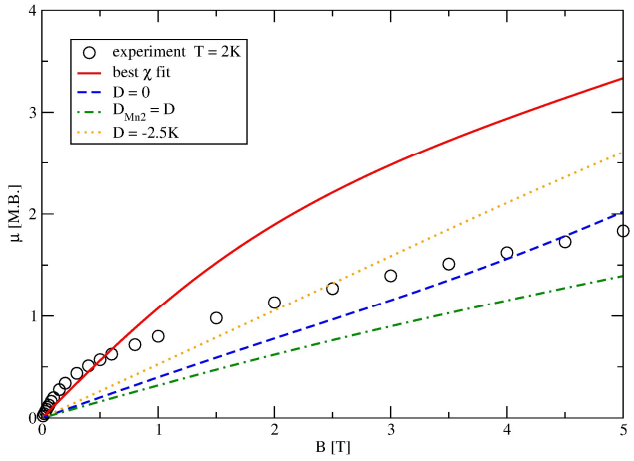


Fig. 6. The magnetic moment per formula unit plotted as a function of the applied field for **1**. The parameters of the theoretical curves are fixed by Eq. (3) except for *D* which is specified in the legend.

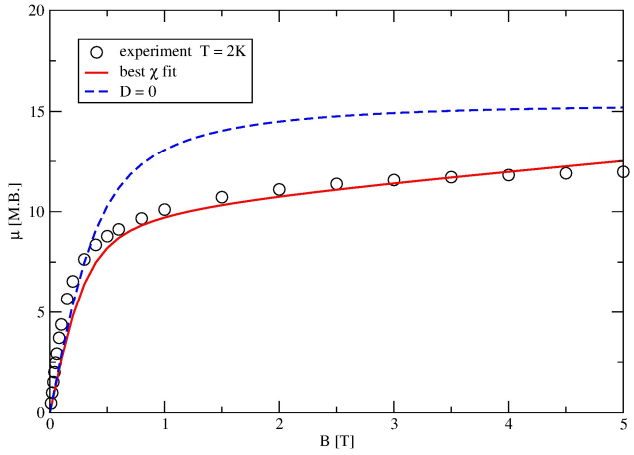


Fig. 7. The magnetic moment per formula unit plotted as a function of the applied field for **2**. The parameters of the theoretical curves are fixed by Eq. (4) except for *D* which is specified in the legend.

The best susceptibility fits are presented in Fig. 4 and Fig. 5 by the red lines. To bring out the effects of the zero-field splitting, we have put the single-ion anisotropy parameters D=0 and have plotted the isotropic counterparts by the blue lines. We see in Fig. 4 that the anisotropy term is needed for **1** to recover a bump in the low temperature region. For the susceptibility behaviour of **2** (see Fig. 5), the role of anisotropy is also visible in the low temperature tail and entails the reduction of $\chi$. More striking evidence of the impact of the anisotropy is demonstrated for the magnetization profiles considered in Figs. 6 and 7.

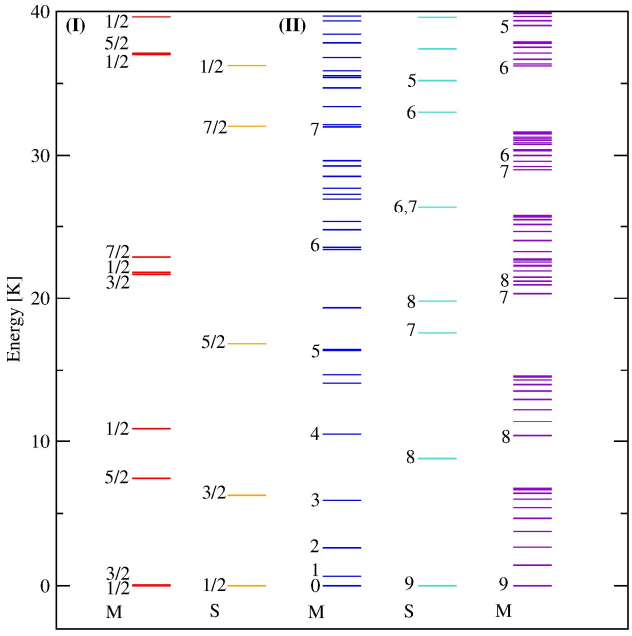


Fig. 8. The energy structure of **1** and **2** shown in panels (I) and (II), respectively. The total spin quantum numbers $S_T$ found in the isotropic limit, and the absolute values $|M_T|$ characterising some energy levels for the models describing **1** and **2**, are indicated in the first four columns labelled by S and M. The last column shows the spectrum predicted for the SMM analogue of **2** with *D*=-0.4.

The zero-field splitting affects the energy structure (Fig. 8) and the low temperature isotherms of magnetization. Their location in Figs. 6 and 7 strongly depends on the parameter *D*. The sizable effect of anisotropy on the magnetization profiles is not surprising as the condition T<*D* is fulfilled for both compounds.[24] The field dependence of the measured T=2 K isotherm for **2** is reproduced quantitatively in the entire field region, using the parameters (4). In the case of **1**, the agreement occurs for weak magnetic fields only, nevertheless this result is valuable due to the volatility of the magnetization profiles directly demonstrated in Fig. 6. This feature indicates that anisotropy is crucial for the shape of the magnetization isotherms and the lack of quantitative agreement with experiment for **1** suggests that it is not represented accurately enough in the model (1).

The values of parameters given in Eqs. (3) and (4) fall correctly into the acceptable range established earlier.[6e,24] For **2**, the value *g*=1.70 seems excessively small, comparing to the corresponding data quoted for the manganese compounds e.g. in Table 24 and 25.[24] However, for the manganese tetramers (e.g. Table 1 in Jerzykiewicz et al., 2010)[6e] such a small *g*-value is not exceptional.

The low energy spectra corresponding to the parameter sets (3) and (4) are illustrated in Fig. 8 in panels (I) and (II), respectively. For **1**, the ground state is a doublet M=±1/2, the gap between the low-lying doublets M=±1/2, ±3/2 is very small and accounts for a fast relaxation to the thermal equilibrium in agreement with the absence of the out-of-phase signal in the dynamic susceptibility.

Dalton Transactions

ARTICLE

The out-of-phase signal is not observed in **2** either, due to the non-magnetic ground state M=0 (see Fig. 8) arising from the positive value of the anisotropy parameter. In such a system, the magnetic ground state can only be induced by an applied field and it is unstable as soon as the field is removed. This feature explains the lack of the $\chi''$ signal despite the ferromagnetic couplings and the expected S=9 ground state.

To discuss the results in terms of the Lieb-Mattis theorem[6g-h] (LMT) and bipartiteness,[7] we have to *neglect the zero-field splitting*. Then a finite system of quantum spins $\mathbf{s}_j$ coupled by isotropic interactions $\mathbf{J}_{jk}\mathbf{s}_j\cdot\mathbf{s}_k$ is bipartite if it can be split into two separable parts A and B, and there exists a real number $\boldsymbol{g}^2$ (which is non-negative) being simultaneously the lower bound for the exchange couplings $\mathbf{J}_{jk}$ between spins from *different* subsystems and the upper bound for interactions between spins within the same sublattices. We assume always that the positive couplings describe the antiferromagnetic interactions. According to this definition of bipartiteness, the compound **1** represented by the model shown in Fig. 3 with the corresponding set of couplings is bipartite with $\boldsymbol{g}^2$=0. This conclusion is justified, by partitioning the spin system into the parts A={1, 3} and B={2, 4}. Then, referring to LMT, we can predict the unique ground state $S_T$=1/2. In fact, the system remains bipartite and its ground state is unchanged if the coupling $J_3$ is antiferromagnetic, provided that $J_3 < \min(J_1, J_2)$.

We state, referring to LMT, that [$Mn^{II}_3Mn^{III}$] core is a very good candidate for a molecular qubit, as the stability of the S=1/2 ground state doublet arises from the bipartiteness of the model in the broad sector of the interaction parameters. As to the [$Mn^{II}Mn^{III}_3$] core (Scheme 1 in M.W. Wemple et al)[6f] with the antiferromagnetic couplings $J_1$ and $J_3$, the existence of the S=1/2 ground state can be predicted from LMT and it is realized for the ratio $J_1/J_3 \geq 0.73$.

Unfortunately, in **1** the zero-field splitting interferes strongly so that the ground state doublet M=±1/2, albeit survives, is barely separated from the higher M=±3/2 level (see Fig. 8). However, the gap Δ increases monotonically from the value 0.06 K for *D*=-4.5 K up to 6.3 K for *D*=0 (see the second column in Fig. 8). We note that the tiny gap found for **1** is probably an artefact of our simplified model because the theoretical magnetization profile overestimates the experimental data in Fig. 6, i.e. there is too strong contribution from the M=3/2 state.

We have also analyzed vulnerability of the gap to a variation of the couplings in the regions consistent with the values found for **1**, assuming that anisotropy vanishes. As illustrated in Fig. 9, the size of the gap monotonically increases with increasing couplings. The most relevant is the dependence on $J_2$, i.e. the coupling between the $Mn^{II}$ ions. The highest gap of the order of 13 K was observed in the $Cr_7Ni$ molecule.[25] In the case of the $Cr_9$ molecule,[6c] the size of the gap was smaller by a factor of 2.5, whereas for **1**, it is squeezed by two orders of magnitude. For the chromium ring analogue of $Cr_9$, the maximal magnitude of the gap 7.5 K was determined.[6c] For the analogue of **1**, the record value 13 K can be overcome if the value $J_2$=2.4 K is enhanced only by a factor of 3 (see Fig. 9).

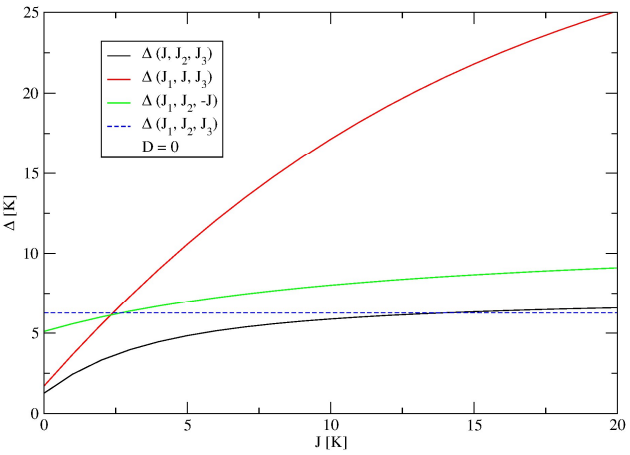


Fig. 9. The dependence of the lowest energy gap Δ on the strength of the parameters chosen for the models of the [$Mn^{II}_3Mn^{III}$] core in the isotropic limit. The values $J_1$, $J_2$, $J_3$ are taken from the set (3). The broken blue line shows the size of the gap precisely for these values and the red line reveals the crucial role of the $Mn^{II}$ – $Mn^{II}$ coupling.

Finally, we emphasize that the compound **2** is another example of the bipartite mixed-valence complex with $\boldsymbol{g}^2$=0. In the case of ferromagnetic couplings $J_1$ and $J_3$, the bipartiteness of **2** is trivial as the subsystem A can be equated with the entire system (Fig. 3) and the subsystem B can be considered empty. This property implies the ground state with the total spin $S_T$=9 which is found in **2**, neglecting the zero-field splitting (see the fourth column in Fig. 8). However, such a complex remains bipartite with $\boldsymbol{g}^2$=0 if the coupling $J_1$ becomes aniferromagnetic and then the total spin $S_T$=1 in the ground state is only allowed. We conclude that LMT explains why for the complexes with the [$Mn^{II}_2Mn^{III}_2$] core (see Table 7 in Zhou et al.[26] and Table 1 in Jerzykiewicz et al. [6e]) the values $S_T$=1 and $S_T$=9 are found. In addition, we have estimated the lower bound *D*=-

0.4 K of the anisotropy parameter which could suppress the strong S-mixing effects and support the SMM behaviour in the analogue of **2**. The energy structure fulfilling these conditions for $D$=-0.4 K is presented in the fifth column in Fig. 8.

In order to validate the phenomenological models, the DFT calculations have been carried out both in the presence and in the absence of the spin-orbit coupling. Details involving DFT calculations performed for both **1** and **2** are described in Computational details section of the Electronic Supplementary Information.

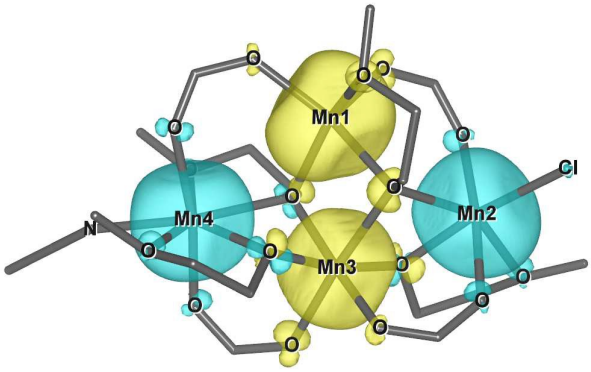


Fig. 10. The spin density maps for **1**. The isosurfaces are plotted for 0.015 e/Bohr$^3$. The colours diversify the directions of the magnetic moments localized on the manganese sites.

Our calculations confirm that the magnetic configuration corresponding to the lowest total energy of **1** is ferrimagnetic. The sharp spin density localization on the manganese sites, shown in Fig. 10, leads to the local magnetic moments in $\mu_B$ equal to 4.39, 4.42, 3.56, 4.44 for Mn1, Mn2, Mn3, Mn4, respectively. These results confirm qualitatively the model (1) and the parameters found. Assuming the proper values of spin, the Landé splitting factors amount to about 1.8. The total energy of the ferromagnetic configuration of the magnetic moments, referred to as the high-spin (HS) configuration, is higher by about 124 meV than that of the ferrimagnetic one. The energy depends slightly on direction of the quantization axis, if the spin-orbit coupling is included which can be attributed to the anisotropic surrounding around the manganese ions. However, the distance between the total energies of the configurations considered is stable within 0.1 meV. Electronic Supplementary Information (Tables S9 and S10) contain detailed values of energies and magnetic moments. We have also attempted to estimate the magnetic couplings within the broken symmetry (BS) approach.[27a-c] Considering the non-equivalent symmetric BS spin configurations listed in Table S9, we have estimated the magnetic couplings from the corresponding energy differences and have obtained: $J_1$=30.4 K, $J_2$=33.4 K, $J_3$=-1.9 K. These values are qualitatively correct only which is not surprising and rather common. Nevertheless, the DFT calculations support the model suggested and the types of interactions present. Moreover, from these qualitative data and LMT, the total spin in the ground state $S_T$=1/2 can be predicted.

In the case of **2**, the DFT predictions are not conclusive. The ground state magnetic configurations depend on direction of the quantization axis. Nevertheless, the spin density is localized on the manganese ions and the local moments amount to 3.6(1) and 4.41(1) in $\mu_B$ for Mn1, Mn3 and Mn2, Mn4, respectively. These findings are consistent with the model (2), as far as the localization of the magnetic moment and Landé factors are concerned.

## Conclusions

Two tetranuclear mixed-valent clusters **1** and **2** containing the cores $[Mn^{II}_3Mn^{III}]$ and $[Mn^{II}_2Mn^{III}_2]$ were synthesized and characterized by physical measurements as well as their models were analyzed within the phenomenological approach and the DFT calculations. Complex **1** is the first example of tetranuclear cluster containing four manganese atoms with the distribution of oxidation states: one Mn(III) and three Mn(II) atoms. Within the spin models considered the quantitative agreement between theory and experiment was achieved for **2**, whereas for **1** the agreement is semi-quantitative but the model predictions are supported by DFT. The complexes exhibit the lowest $S_T$=1/2 and the highest $S_T$=9 possible values of the total spin in the ground states, which are desirable prerequisites for the molecular qubits and SMMs, respectively. Both compounds provide examples of the bipartite spin systems so that LMT implies the ground state degeneracy and architecture of their low-energy level structure. The topology of interactions in **1** with the magnetic core $[Mn^{II}_3Mn^{III}]$ is suitable for synthesis of molecules with the ground state $S_T$=1/2 and the lowest energy gap higher than that observed in the chromium-based molecules.

## Acknowledgements

The authors thank Dr. B. Brzostowski, Dr. W. Florek and Dr. A. Bieńko for helpful discussions. This work was supported in part by the National Science Center (Poland) within the project No N202 230137. We acknowledge access to the HPC resources in PSNC Poznań (Poland) and those available within the DECI program by PRACE-3IP project (FP7 RI-312763) as well as computing servers in the Institute of Physics at University of Zielona Góra. Furthermore, one of the authors (M. W.) was supported by the European Union scholarship No DFS.VI.052.4.62.8.2013 from Human Capital Programme, sub-measure 8.2.2, priority VIII, funded from EFS and the Lubusz Voivodeship budget.

## Notes and references

1 N. Harden, M. A. Bolcar, W. Wernsdorfer, K. A. Abboud, W. E. Streib and G. Christou, *Inorg. Chem*., 2003, **42**, 7067.
2 H. Miyasaka, R. Clérac, W. Wernsdorfer, L. Lecren, C. Bonhomme, K. Sugiura and M. Yamashita, *Angew. Chem*., 2004, **116**, 2861.
3 R. Sessoli, H. L. Tsai, A. R. Schanke, S. Wang, J. B. Vincent, K. Folting, D. Gatteschi, G. Christou and D. N. Hendrickson, *J. Am. Chem. Soc*., 1993, **115**, 1804.
5. (a) L. M. Wittick, K. S. Murray, B. Moubaraki, S. R. Batten, L. Spiccia and K. J. Berry, *Dalton Trans*., 2004, 1003. (b) C. I. Yang, G. H. Lee, C. S. Wur, J. G. Lin andH. L. Tsai, *Polyhedron*, 2005, **24**, 2215. (c) L. Lecren, O. Roubeau, C. Coulon, Y. G. Li,

Dalton Transactions

ARTICLE

X. F. Le Goff, W. Wernsdorfer, H. Miyasaka and R. Clérac, *J. Am. Chem. Soc.*, 2005, **127**, 17353. (d) A. M. Ako, V. Mereacre, I. J. Hewitt, R. Clérac, L. Lecren, C. E. Anson and A. K. Powell, *J. Mater. Chem.*, 2006, **16**, 2579. (e) ) L. Lecren, O. Roubeau, Y. G. Li, X. F. Le Goff, H. Miyasaka, F. Richard, W. Wernsdorfer, C. Coulon and R. Clérac, *Dalton Trans.* 2008, 755.

6. (a) G. A. Timco, S. Carretta, F. Troiani, F. Tuna, R. J. Pritchard, C. A. Muryn, E. J. L. McInnes, A. Ghirri, A. Candini, P. Santini, G. Amoretti, M. Affronte, and R. E. P. Winpenny, *Nat. Nanotechnology*, 2009, **4**, 173. (b) M. L. Baker, G. A. Timco, S. Piligkos, J. S. Mathieson, H. Mutka, F. Tuna, P. Kozłowski, M. Antkowiak, T. Guidi, T Gupta, H. Rath, R. J. Woolfson, G. Kamieniarz, R. G. Pritchard, H. Weihe, L. Cronin, G. Rajaraman, D. Collison, E. J. L. McInnes, and R. E. P. Winpenny, *Proc. Natl. Acad. Sci. USA*, 2012, **109** ,19113. (c) M. Antkowiak, P. Kozłowski, G. Kamieniarz, G.A. Timco, F. Tuna, and R.E.P. Winpenny, *Phys. Rev.*, 2013, **B87**, 184430. (d) A. J. Zhou, J. L. Liu, R. Herchel, J. D. Leng and M. L. Tong, *Dalton Trans*., 2009, 3182. (e) 15 L.B. Jerzykiewicz, J. Utko, M. Duczmal, P. Starynowicz, P. Sobota, Eur. J. Inorg. Chem., 2010, 4492. (f) M. W. Wemple, S. Wang, H. L. Tsai, J. P. Claude, W. E. Streib, J. C. Huffman, G. Christou, D. N. Hendrickson, Inorg. Chem., 1996, **35**, 6437. (g) E. Lieb, T. Schultz and D. Mattis, *Ann. Phys.* (N.Y), 1961, **16**, 407. (h) E. Lieb and D. Mattis, *J. Math. Phys.* 1962, **3**, 749. (i) J. Schnack, *Dalton Trans.*, 2010, **39**, 4677. (j) P. Kozłowski, *Phys. Rev.*, 2015, **B91**, 174432.
7. G. Kamieniarz, W. Florek, M. Antkowiak, Phys. Rev., 2015, **B92**, 140411(R).
8. H. Dau, I. Zaharieva and M. Haumann, *Current Opinion in Chemical Biology*, 2012, **16**, 3.
9. (a) Y. Umena, K. Kawakami, J. R. Shen and N. Kamiya, *Nature*, 2011, **473**, 55. (b) M. Suga, F. Akita, K. Hirata, G. Ueno, H. Murakami, Y. Nakajima, T. Schimizu, K. Yamashita, M. Yamamoto, H. Ago, J.R. Shen, *Nature*, 2015, **517**, 99.
10. D. Huang, X. Zhang, C. Ma, H. Chen, C. Chen, Q. Liu, C. Zhang, D. Liao and L. Li, *Dalton Trans.*, 2007, 680.
11. E. K. Brechin, J. Yoo, M. Nakano, J. C. Huffman, D. N. Hendrickson and G. Christou, *Chem. Commun*., 1999, 783.
12. (a) J. Yoo, A. Yamaguchi, M. Nakano, J. Krzystek, W. E. Streib, L. C. Brunel, H. Ishimoto, G. Christou and D. N. Hendrickson, *Inorg. Chem*., 2001, **40**, 4604. (b) D. J. Price, S. R. Batten, K. J. Berry, B. Moubaraki and K. S. Murray, *Polyhedron*, 2003, **22**, 165. (c) C. I. Yang, G. H. Lee, C. S. Wur, J. G. Lin andH. L. Tsai, *Polyhedron*, 2005, **24**, 2215. (d) L. Lecren, Y. G. Li, W. Wernsdorfer, O. Roubeau, H. Miyasaka and R. Clérac, *Inorg. Chem. Commun.*, 2005, **8**, 626. (e) L. Lecren, W. Wernsdorfer, Y. G. Li, O. Roubeau, H. Miyasaka, and R. Clérac, *J. Am. Chem. Soc*., 2005, **127**, 11311. (f) H. Miyasaka, K. Nakata, L. Lecren, C. Coulon, Y. Nakazawa, T. Fujisaki, K. I. Sugiura, M. Yamashita and R. Clérac, *J. Am. Chem. Soc.*, 2006, **128**, 3770. (g) T. C. Stamatos, K. M. Poole, K. A. Abboud, W. Wernsdorfer, T. A. O'Brien and G. Christou, *Inorg. Chem*., 2008, **47**, 5006. (h) K. J. Heroux, H. M. Quddusi, J. Liu, J. R. O'Brien, M. Nakano, E. del Barco, S. Hill and D. N. Hendrickson, *Inorg. Chem*., 2011, **50**, 7367. (i) A. Saha, K. A. Abboud and G. Christou, *Inorg. Chem*., 2011, **50**, 12774. (j) T. C. Stamatos, R. Adam, C. P. Raptopoulu, V. Psycharis, R. Ballesteros, B. Abarca, S. P. Perlepes and A. K. Boudalis, *Inorg. Chem. Commun*., 2012, **15**, 73. (k) C. Y. Shao, L. L. Zhu and P. P. Yang, *Z. Anorg. Allg. Chem*., 2012, **638**, 1307. (l) T. N. Nguyen, K. A. Abboud and G. Christou, *Polyhedron*, 2013, **66**, 171.
13. (a) L. M. Wittick, L. L. Jones, P. Jensen, B. Moubaraki, L. Spiccia, K. J. Berry and K. S. Murray, *Dalton Trans*., 2006, 1534. (b) G. Karotsis, S. J. Teat, W. Wernsdorfer, S. Piligkos, S. J. Dalgarno and E. K. Brechin, *Angew. Chem. Int. Ed*., 2009, **48**, 8285. (c) S. K. Langley, N. F. Chilton, M. Massi, B. Moubaraki, K. J. Berry and K. S. Murray, *Dalton Trans*., 2010, **39**, 7236.
14. L. B. Jerzykiewicz, J. Utko, M. Duczmal and P. Sobota, *Dalton Trans*., 2007, 825.
15. Oxford Diffraction (2009). *CrysAlis PRO*. Oxford Diffraction Ltd, Yarnton, England.
16. R. C. Clark and J. S. Reid, *Acta Cryst*., 1995, **A51**, 887.
17. G. M. Sheldrick, *Acta Cryst*., 2008, **A64**, 112.
18. G. M. Sheldrick, *Acta Cryst.,* 2015, **C71**, 3.
19. G. A. Bain, J. F. Berry, *J.Chem.Educ.*, 2008, **85**, 532.
20. I. D. Brown, *Acta Cryst*., 1992, **B48**, 553.
21. E. C. Yang, N. Harden, W. Wernsdorfer, L. Zakharov, E. K. Brechin, A. L. Rheingold, G. Christou and D. N. Hendrickson, *Polyhedron*, 2003, **22**, 1857.
22. I.J. Bruno, J.C. Cole, P.R. Edgington, M. Kessler, C.F. Macrae, P McCabe, J. Pearson and R. Taylor, *Acta Cryst*., 2002, **B58**, 389.
23. (a) G. Kamieniarz, R. Matysiak, W. Florek, S. Wałcerz, *J. Magn. Magn. Mat.*, 1999, **203**, 271. (b) G. Kamieniarz, M. Haglauer, G. Musial, A. Caramico D'Auria, F. Esposito, D. Gatteschi, *Inorg. Chim. Acta*, 2007, **360**, 3941. (c) G. Kamieniarz, P. Kozłowski, M. Antkowiak, P. Sobczak, T. Ślusarski, D. M. Tomecka, A. Barasiński, B. Brzostowski, A. Drzewiński, A. Bieńko, J. Mroziński, *Acta Phys. Polon*. 2012, **A121**, 992.
24. R. Boča, *Coord. Chem. Rev.*, 2004, **248**, 757.
25. F. Troiani, A. Ghirri, M. Affronte, S. Carretta, P. Santini, G. Amoretti, S. Piligkos, G. Timco, R.E.P. Winpenny, *Phys. Rev. Lett.*, 2005, **94**, 207208.
26. A.-J. Zhou, J.-L. Liu, R. Herchel, J.-D. Leng, M.-L.Tong, *Dalton Trans*., 2009, 3182.
27. (a) L.J. Noodleman, *J. Chem. Phys.,* 1981, **74,** 5737. (b) B. Brzostowski, R. Lemański, T. Ślusarski, D. Tomecka and G. Kamieniarz, *J. Nanopart. Res.,* 2013, **15**, 1528. (c) I. Rudra, Q. Qin and T.v. Voorhis, *Inorg. Chem.*, 2007, **46**, 10539.

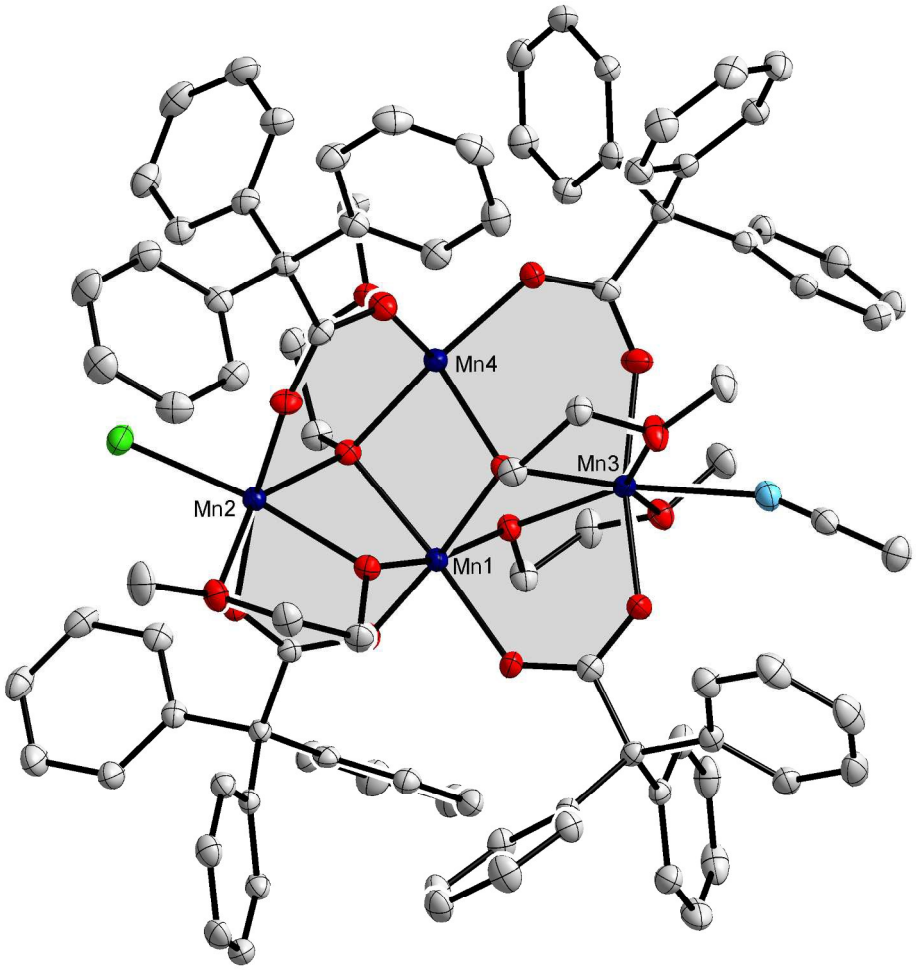


610x624mm (96 x 96 DPI)